A Classification of Binary Tropical Cyclone–Like Vortex Interactions*

RICARDO PRIETO

Centro de Ciencias de la Atmósfera, Universidad Nacional Autónoma de México, Mexico City, Mexico

BRIAN D. MCNOLDY

Department of Atmospheric Science, Colorado State University, Fort Collins, Colorado

SCOTT R. FULTON

Department of Mathematics and Computer Science, Clarkson University, Potsdam, New York

WAYNE H. SCHUBERT

Department of Atmospheric Science, Colorado State University, Fort Collins, Colorado

(Manuscript received 3 December 2002, in final form 14 April 2003)

ABSTRACT

The interaction between two tropical cyclones with different core vorticities and different sizes is studied with the aid of a nondivergent barotropic model, on both the f plane and the sphere. A classification of a wide range of cases is presented, using the Dritschel–Waugh scheme, which subdivides vortex interactions into five types: elastic interaction, partial straining out, complete straining out, partial merger, and complete merger. The type of interaction for a vortex pair on the f plane, and the same pair on the sphere, was the same for 77 out of 80 cases studied. The primary difference between the results on the f plane and those on the sphere is that the vorticity centroid of the pair is fixed on the f plane but can drift a considerable distance poleward and westward on the sphere. In the spherical case, the interaction between the cyclone pair and the associated β-induced cyclonic and anticyclonic circulations can play an important role.

The ''partial merger'' regime is studied in detail. In this regime the interaction between vortices can lead to episodic exchanges of vorticity, with both vortices surviving and entering a stage of continued but weaker interaction. With the aid of passive tracers, it is found that the exchange of vorticity is restricted to the vortex periphery even when the vorticity field within each vortex is flat, so that the vortex core is the last region to be eroded. It is hypothesized that some observed interacting tropical cyclones actually do undergo this partial-merger process.

1. Introduction

An interesting tropical cyclone binary interaction occurred in the east Pacific during September 2001. The event began when Tropical Depression 8 formed on the morning of 4 September. Just 12 h later, it was upgraded to Tropical Storm Gil and was tracking westward. Lagging just a few hours and 1500 km behind Gil was Tropical Depression 9, which would later become Tropical Storm Henriette. Henriette was also tracking westward but moving 50% faster than Gil. On the morning of 6 September, Gil had reached hurricane strength, and, at about the same time, Henriette had reached tropical storm strength. Gil was a relatively compact, intense circulation (42 m s^{-1} peak intensity), while Henriette was a broader, weaker circulation (22 m s^{-1} peak intensity). Figure 1a is a *GOES-10* visible image of these two storms on 6 September 2001 at 2100 UTC. (*GOES-10* visible loops for 6–9 September are available in a supplement found online at http://ams.allenpress.com/amsonline/?request=index-html.)

By the morning of 8 September, the separation between the two vortices had decreased to only 400 km, and signs of vortex interaction began to appear (strong shear aloft and a low-level horizontal convergence band). Also around this time, Henriette had lost strength and was no longer classified as a tropical depression. On the afternoon of 9 September, the centers

* Supplemental information related to this paper is available online (DOI:10.1175/MWR2610Supl1). For current information see http://dx.doi.org/10.1175/MWR2610Supl1.

Corresponding author address: Dr. Ricardo Prieto, Instituto Mexicano de Tecnologia del Agua, Paseo Cuauhnahuac 8532, Jiutepec, Mor. 62550, Mexico.
E-mail: rprieto@tlaloc.imta.mx

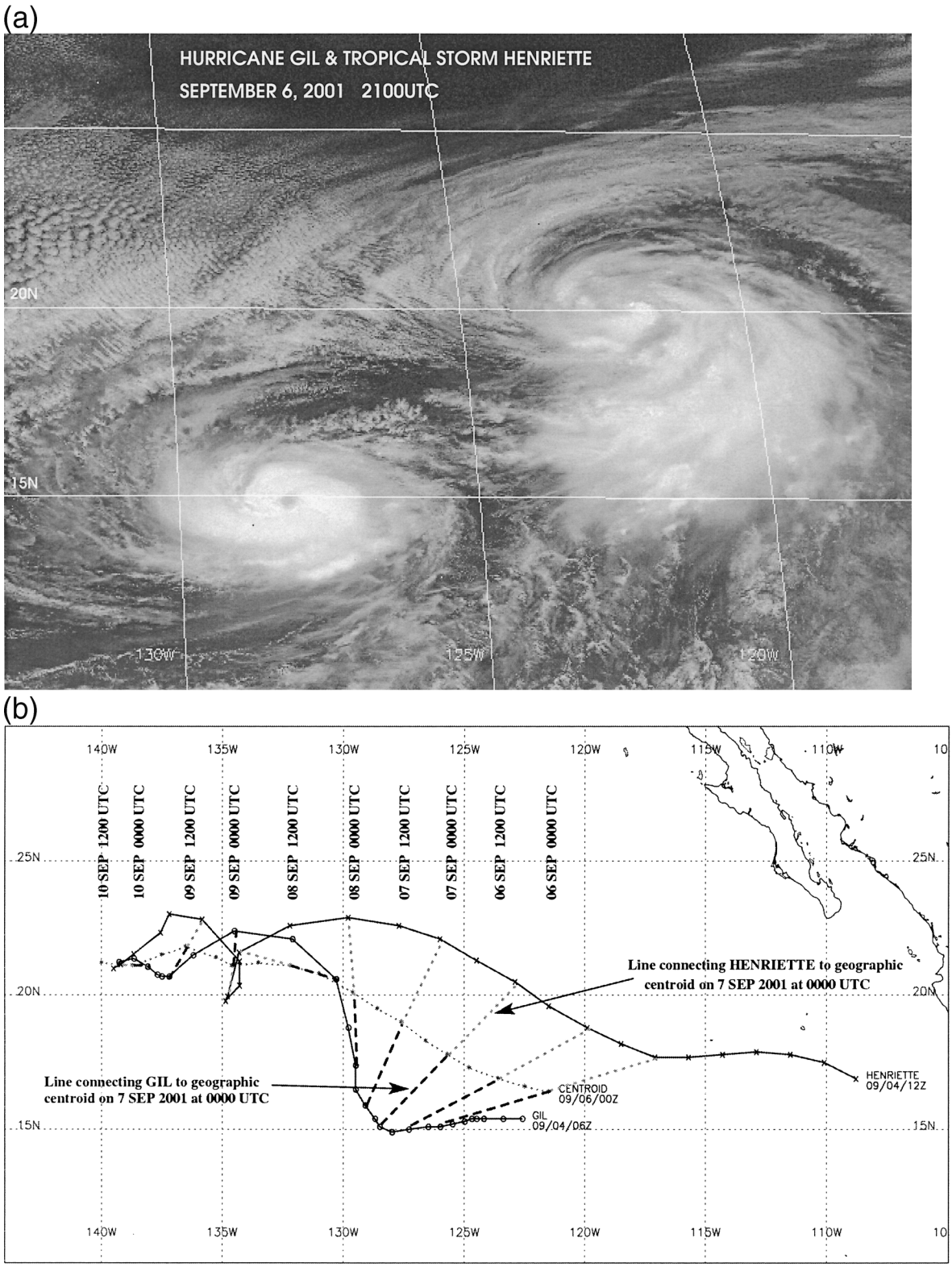

FIG. 1. (a) *GOES-10* visible image of Hurricane Gil and Tropical Storm Henriette at 2100 UTC 6 Sep 2001. Henriette is to the northeast. Latitude and longitude lines are 5° apart, and Gil is at 15°N, 128°W. (b) Tracks of Gil and Henriette based on NHC best-track positions and *GOES-10* visible imagery, shown with their geographic centroid (dashed line).

of Gil and Henriette had come to within 85 km of each other, already having rotated 540° about their centroid. By this time, Gil was also no longer a tropical depression. Finally, by the morning of 10 September, the vortices had merged, with the more compact, intense one (remnants of Gil) victorious. The storm tracks, based on National Hurricane Center (NHC) best-track positions and *GOES-10* visible imagery, are shown in Fig. 1b. This figure shows the geographic centroid; the vorticity centroid could be closer to the stronger storm but cannot be computed without the detailed vorticity field.

The binary vortex interaction is also known as the ''Fujiwhara effect'' in honor of the pioneering work of Fujiwhara (1921, 1923, 1931), who performed a series of laboratory experiments on the interactions between pairs of vortices in a water tank. The interaction of Gil and Henriette is one example of the many cases of binary tropical cyclone interactions that have been documented in the literature (e.g., see Larson 1975; Chang 1983; Lander and Holland 1993; Kuo et al. 2000; Wu et al. 2003). In an early observational study of the interaction of binary tropical cyclones in the western North Pacific, Brand (1970) found that a definitive mutual interaction, in the form of a cyclonic orbit of the storms about their centroid, occurred when the cyclone centers came within 1300 km, and that mutual attraction occurred when the cyclone centers came within 750 km. Of course, these should be regarded as rough forecasting rules since tropical cyclones vary widely in their sizes and strengths. In the western North Pacific the frequency of such binary interactions is approximately 1.5 per year. The frequency of actual merger is lower.

The interaction of two isolated vortices has been examined in detail in a numerical study by Dritschel and Waugh (1992) in which the vortices are patches with equal vorticity, and the radius ratio and separation distance are experimental parameters. The calculations, performed on the f plane using the contour surgery algorithm (Dritschel 1988), show that the interaction of unequal vortices is much richer than that of equal vortices. The interactions can be classified into five different regimes, based upon a quantification of the final to initial circulation of each vortex: (i) elastic interaction, (ii) partial straining out, (iii) complete straining out, (iv) partial merger, and (v) complete merger. These interactions may result in the total destruction of one of the vortices (iii and v), the partial destruction of one vortex (ii and iv), or an interaction in which both vortices survive with their initial circulation (i). These results also imply that the interaction of same-sign vortices is an essential mechanism for vortex growth, as well as an important mechanism for the production of small vortices and for the destruction of vortices.

In another numerical study, Holland and Dietachmayer (1993) investigated the effect of variable Coriolis parameter on the interaction between two tropical cyclones, concluding that the development of ''β gyres'' can have an important impact on the vortex interaction. The β-gyres are the result of the meridional advection of planetary vorticity around a vortex, which induces an asymmetric circulation capable of driving the vortex. β-gyres of sufficient intensity can extend the distance at which one vortex is able to capture the other, or they can produce the escape mode discussed by Lander and Holland (1993).

TABLE 1. Grid parameters at $t = 0$: grid number (l), number of grid points in x and y (n_x, n_y), grid origin (x_0, y_0), grid spacing in x and y (h_l), and time step (Δt_l).

l	n_x	n_y	x_0 (km)	y_0 (km)	h_l (km)	Δt_l (s)
1	512	512	−5223.63	−4613.87	20.4048	450.00
2	512	512	−2611.82	−2614.19	10.2024	225.00
3	512	512	−1305.91	−1308.29	5.1012	112.50
4	512	512	−652.95	−655.33	2.5506	56.25

From the theoretical point of view, Melander et al. (1986) developed a vortex interaction model by considering the evolution of finite-area, uniform-vorticity regions in an unbounded inviscid fluid. Their analysis of the two-dimensional Euler equations results in a system of ordinary differential equations governing the physical-space moments of the individual regions. Truncation of this infinite system yields an nth-order moment model. In the second-order model each region is assumed to be elliptical, and the equations of motion conserve local area, global centroid, total angular impulse, and global excess energy. The model forms a Hamiltonian system, with the excess energy as the Hamiltonian. This model can crudely describe the collapse of two vortex centers. However, as the vortex centers approach during merger, the model becomes increasingly invalid because it assumes that an elliptical shape is maintained throughout the process.

Another theory of vortex merger has been presented by Lansky et al. (1997). In their theory, a point vortex and an extended vortex of nearly circular cross section interact. The general behavior of this system involves the rotation of the point vortex around the extended vortex, together with finite-amplitude oscillations in the radial direction. The radial motion of the point vortex is trapped inside a critical layer of characteristic width. Lansky et al. (1997) found that if the total circulation of the point vortex divided by the total circulation of the extended vortex exceeds a critical value, there is an overlap of neighboring critical layers around the extended vortex, having as a consequence the cascade of the point vortex through a sequence of resonances as it spirals in and merges with the extended vortex.

Ritchie and Holland (1993) estimated the critical separation distance between two atmospheric vortices for merger to occur. They assumed that once one of the

vortices produces a strain large enough to result in a significant distortion of the other vortex, mutual rotation between vortices breaks down and shearing out of one vortex or merger occurs. For typical tropical cyclone parameters, Ritchie and Holland (1993) found that the vortices must come to within 150–300 km before the merger or shearing-out process can start.

In this paper we use numerical results from a barotropic model to explore the range of possible binary interactions between tropical cyclones. In doing so we extend the work of Dritschel and Waugh (1992) by considering vortices of different strengths and sizes and by examining the effects of geometry (f plane versus sphere). The paper is organized in the following way: First, the multigrid barotropic model (MUDBAR) is described (section 2). After specifying the family of initial conditions (section 3), the MUDBAR model is then used (section 4) to simulate a broad range of binary interactions in which the parameters are the relative size of the storms, their separation distance, and the relative vorticity ratio between them. We then discuss (section 5) the differences between interactions on the f plane and the sphere. Finally, a summary of the results and conclusions is presented (section 6).

2. The MUDBAR numerical model

The numerical model used in all our experiments is the MUDBAR model described by Fulton (1997, 2001). The model is formulated on a section of the spherical earth. Using spherical coordinates (λ, ϕ), the governing vorticity equation and invertibility principle are

$$\frac{\partial \zeta}{\partial t} + \frac{\partial(\psi, \zeta)}{a^2 \partial(\lambda, \sin\phi)} + \frac{2\Omega}{a^2}\frac{\partial \psi}{\partial \lambda} = \nu\left[\frac{\partial^2 \zeta}{a^2 \cos^2\phi \partial\lambda^2} + \frac{\partial}{a \cos\phi \partial\phi}\left(\cos\phi \frac{\partial \zeta}{a\partial\phi}\right)\right], \quad (1)$$

$$\frac{\partial^2 \psi}{a^2 \cos^2\phi \partial\lambda^2} + \frac{\partial}{a \cos\phi \partial\phi}\left(\cos\phi \frac{\partial \psi}{a\partial\phi}\right) = \zeta, \quad (2)$$

where a is the earth's radius, Ω the earth's rotation rate, ν the constant diffusion coefficient, ζ the relative vorticity, and ψ the streamfunction. In the present study a transformation of (1) and (2) to Mercator coordinates has the important advantage of allowing us to easily obtain the f-plane version of the model by a simple parameter change. The transformation from the spherical coordinates (λ, ϕ) to the Mercator coordinates (x, y) is given by $x = (\lambda - \lambda_0)a\cos\phi_0$ and $y = [\tanh^{-1}(\sin\phi) - \tanh^{-1}(\sin\phi_0)]a\cos\phi_0$, where the reference point (λ_0, ϕ_0) coincides with the origin of the Mercator coordinate system. After transformation to Mercator coordinates, the model equations (1) and (2) take the form

$$\frac{\partial \zeta}{\partial t} + m^2\frac{\partial(\psi, \zeta)}{\partial(x, y)} + \beta\frac{\partial \psi}{\partial x} = \nu m^2\left(\frac{\partial^2 \zeta}{\partial x^2} + \frac{\partial^2 \zeta}{\partial y^2}\right), \quad (3)$$

$$m^2\left(\frac{\partial^2 \psi}{\partial x^2} + \frac{\partial^2 \psi}{\partial y^2}\right) = \zeta, \quad (4)$$

where $\beta = a^{-1}2\Omega\cos\phi_0$ and $m = \cos\phi_0/\cos\phi$ is the map factor. Since (3) and (4) are exact transformations of (1) and (2), the full effects of the earth's sphericity are included in (3) and (4) when we use $\beta = a^{-1}2\Omega\cos\phi_0$ and $m = \cos\phi_0/\cos\phi$. However, if we set $\beta = 0$ and $m = 1$ in (3) and (4), we discard all spherical effects and obtain the f-plane model. As a third alternative, the choice to use $\beta = a^{-1}2\Omega\cos\phi_0$ and $m = 1$ results in the β-plane model. For the flow patterns studied here, the β-plane model gives results that are qualitatively similar to those of the full spherical model, so we have chosen to present only the results from the full spherical model and the f-plane model.

The model domain is a rectangle in x and y centered at $(x, y) = (0, 0)$, where $(\lambda_0, \phi_0) = (60°\text{W}, 20°\text{N})$. For most of our integrations we have used four nested grids, each with 512×512 points. For the integrations on the sphere, the outermost grid extends 100° in the east–west direction and extends from 60.8°N to 21.5°S in the north–south direction. At the boundaries the normal flow is assumed to vanish. The space discretization uses fourth-order finite differences on uniform rectangular grids; in particular, the second term in (3) is approximated by the fourth-order Arakawa Jacobian. The time discretization uses a fourth-order Runge–Kutta scheme. A summary of the grid parameters is given in Table 1. For the diffusion coefficient we have chosen $\nu = 250\ \text{m}^2\ \text{s}^{-1}$. For a more detailed description of the model, the reader is referred to Fulton (1997, 2001).

3. Initial conditions

The observed vorticity profile in intensifying hurricanes (Kossin and Schubert 2001) can be described as a thin annulus of strongly enhanced vorticity embedded in nearly irrotational flow. This is a highly unstable configuration that tends to break down and relax toward a vorticity monopole (Schubert et al. 1999; Kossin and Schubert 2001). Because the vorticity peak of the hurricane core is much higher than the vorticity of the immediately surrounding flow, we may consider the hurricane, to a first approximation, as a vorticity patch. For this work, we consider initial conditions that consist of two circular patches of uniform vorticity with sharp edges. The size of vortex 1 is fixed, while the size of vortex 2 is a variable parameter. The separation distance between the vortices is also a variable parameter. The precise mathematical form of the initial condition is $\zeta(x, y, 0) = \zeta^{(1)}(x, y) + \zeta^{(2)}(x, y)$, where

$$\zeta^{(j)}(x, y) = \zeta_j \begin{cases} 1, & 0 \le r_j(x, y) \le R_j - d \\ S\left(\dfrac{r_j(x, y) - R_j + d}{2d}\right), & R_j - d \le r_j(x, y) \le R_j + d \\ 0, & R_j + d \le r_j(x, y) < \infty \end{cases}$$

for $j = 1, 2$, with $r_j(x, y) = [(x - x_j)^2 + y^2]^{1/2}$, $d = 15$ km, $S(r) = 1 - 3r^2 + 2r^3$, $R_1 = 100$ km, and R_2 a variable parameter. The separation distance between the vortex centers is $x_2 - x_1$, while the separation distance between their edges, measured from the centers of the skirt regions, is defined as $\Delta = x_2 - x_1 - (R_1 + R_2)$. Initially, vortex 1 is to the left of vortex 2, with the constants ζ_1 and ζ_2 giving the vorticities at the cores of vortex 1 and vortex 2, respectively.

Initially, each vortex was uniformly covered with passive tracers, and the trajectories of these tracers were calculated during the entire evolution of each experiment. In order to classify the type of vortex interaction, the ratio of final to initial circulation was estimated for each of the two vortices with the aid of the computed trajectories. We associated a circulation value with each of the parcels so the sum of all the parcels' ''circulations'' within a vortex is equal to the vortex circulation. We use Dritschel and Waugh's (1992) classification of the different flow regimes:

1) elastic interaction (EI): $\hat{C}_1 = 1$, $\hat{C}_2 = 1$;
2) partial straining out (PSO): $\hat{C}_1 = 1$, $\hat{C}_2 < 1$;
3) complete straining out (CSO): $\hat{C}_1 = 1$, $\hat{C}_2 = 0$;
4) partial merger (PM), $\hat{C}_1 > 1$, $\hat{C}_2 < 1$; and
5) complete merger (CM), $\hat{C}_1 > 1$, $\hat{C}_2 = 0$;

where $\hat{C}_1 = C_{1f}/C_{1i}$ and $\hat{C}_2 = C_{2f}/C_{2i}$ denote the ratio of the final to the initial circulation for each vortex.

4. Results of the numerical experiments

Consider first the case in which the vorticity ratio is $\zeta_2/\zeta_1 = 0.6$ and the core vorticity in the left vortex is $\zeta_1 = 9.33 \times 10^{-4}$ s^{-1}, which gives a maximum wind speed at its edge of $v_{\max} = 46.7$ m s^{-1} (a strong category 2 hurricane on the Saffir–Simpson scale). The strength of the vortex on the right depends on the value of the parameter R_2. For $R_2 = R_1 = 100$ km, the maximum wind speed of vortex 2 is 28.0 m s^{-1}, which corresponds to tropical-storm-force winds. For the case $\zeta_2/\zeta_1 = 0.6$, a total of 40 experiments were performed on the f plane, with R_2 ranging from 25 to 200 km in increments of 25 km, and Δ ranging from 50 to 250 km in increments of 50 km. All the experiments were run for 72 h, which is long enough to provide a classification of the interaction. Figure 2 shows five cases that illustrate the different types of interactions: (a) is a complete merger ($\Delta/R_1 = 1.0$, $R_2/R_1 = 1.50$); (b) is a partial merger ($\Delta/R_1 = 2.0$, $R_2/R_1 = 1.75$); (c) is a complete straining out ($\Delta/R_1 = 1.5$, $R_2/R_1 = 0.50$); (d) is a partial straining out ($\Delta/R_1 = 2.0$, $R_2/R_1 = 0.75$); and (e) is an elastic interaction ($\Delta/R_1 = 2.5$, $R_2/R_1 = 1.25$). The times shown in Fig. 2 vary from case to case and have been selected to demonstrate the key interactions during the flow evolution. All the panels have the same spatial scales to allow for a direct comparison, and the display of tracers has been omitted for clarity. The classification of the 40 f-plane experiments with $\zeta_2/\zeta_1 = 0.6$ is shown by the color codes in the top surface shown in Fig. 3.

A general feature of this series of experiments is the dominance of the stronger vortex (black shading in Fig. 2), which rolls up all or part of the weaker vortex when the two are close enough to allow for an inelastic interaction. Two out of the five interaction types (CM and CSO) result in the destruction of the weaker vortex. The other three types of interaction (PM, PSO, and EI) end up with two vortices, although one of the vortices may have considerably reduced circulation. At $t = 72$ h, all the experiments have a somewhat more complicated flow than their initial condition because of the presence of filaments and the deformation of the initially circular vortex shapes. We discuss the partial-merger case, shown in Fig. 2b, in more detail in section 5.

For the case in which $\zeta_2/\zeta_1 = 0.8$, we expect a less-dominant behavior of the stronger vortex than when $\zeta_2/\zeta_1 = 0.6$. The vortex initially on the left has a vorticity $\zeta_1 = 7.0 \times 10^{-4}$ s^{-1} with a radius $R_1 = 100$ km, which produces a maximum wind speed of 35 m s^{-1} (a weak category 1 hurricane on the Saffir–Simpson scale). The vorticity of vortex 2 is $\zeta_2 = 5.6 \times 10^{-4}$ s^{-1}, which is the same vorticity as the weaker vortex in the $\zeta_2/\zeta_1 = 0.6$ case. For the case $R_2 = 100$ km, vortex 2 has tropical-storm-force winds of 28 m s^{-1}. For the $\zeta_2/\zeta_1 = 0.8$ case, we have performed another 40 experiments varying the size of vortex 2 (R_2) and the separation distance (Δ), as in the $\zeta_2/\zeta_1 = 0.6$ case. The classification of these 40 f-plane experiments with $\zeta_2/\zeta_1 = 0.8$ is shown by the color codes in the middle surface of Fig. 3.

The bottom surface shown in Fig. 3 has been adapted from the work of Dritschel and Waugh (1992, their Fig. 5) and is for the case $\zeta_2/\zeta_1 = 1.0$. Note that when $\zeta_2/\zeta_1 = 1.0$, the information given in the region $0 \le R_2/R_1 \le 1$ is redundant with the information given in the region $1 \le R_2/R_1 < \infty$ since the vortex subscripts 1 and 2 can be interchanged. In studying Fig. 3, one should also note that the numerical values for the radius ratio R_2/R_1 and nondimensional separation distance Δ/R_1 on the bottom surface apply to all three surfaces, but that

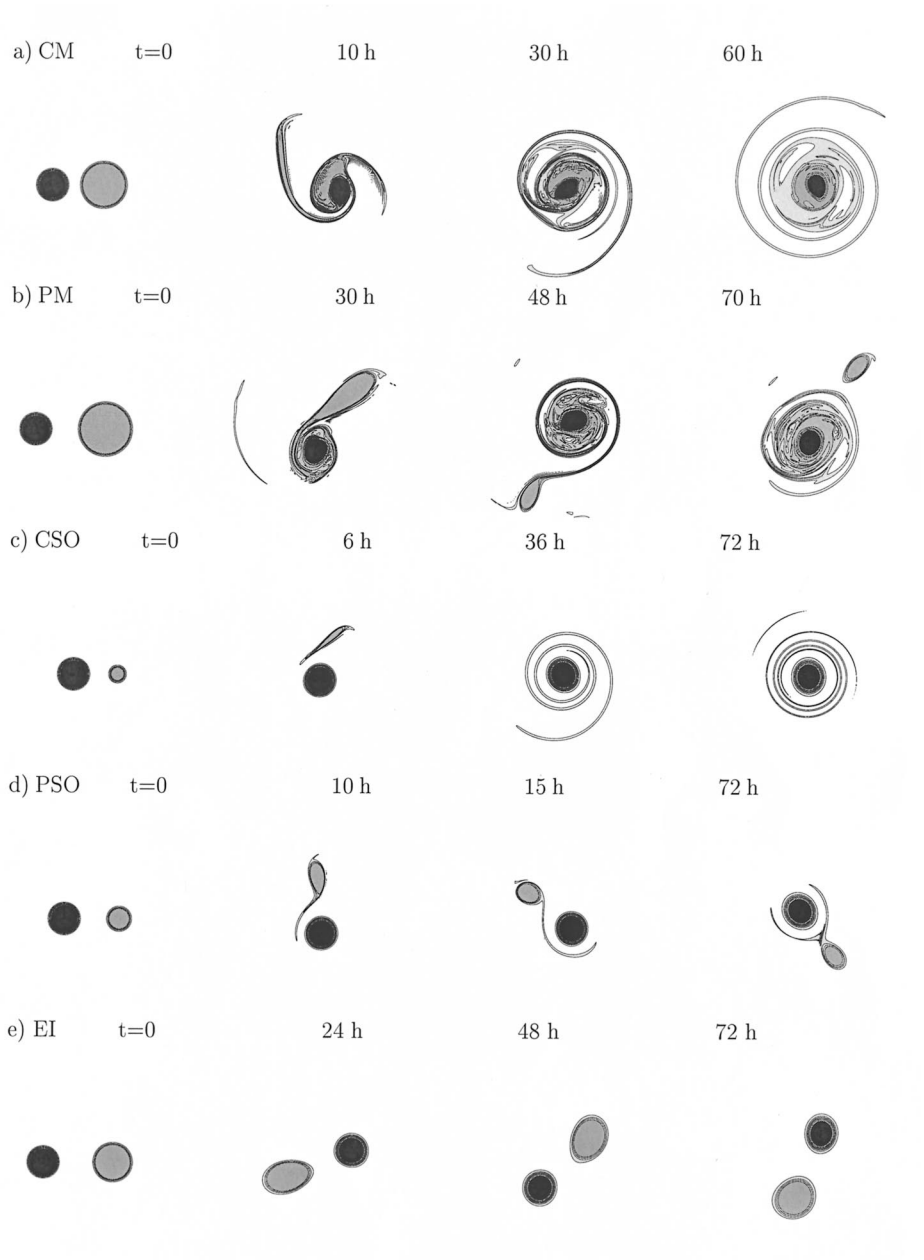

FIG. 2. Vorticity field at selected times showing different classifications of binary vortex interactions on the f plane: (a) complete merger (CM), (b) partial merger (PM), (c) complete straining out (CSO), (d) partial straining out (PSO), and (e) elastic interaction (EI). At $t = 0$, the vortices are patches of constant vorticity with sharp edges. Black shading indicates $\zeta_1 = 9.33 \times 10^{-4}\ \mathrm{s}^{-1}$ and gray shading indicates $\zeta_2 = 0.6\zeta_1$.

the numerical values for the circulation ratio C_2/C_1 are different for each surface.

From Fig. 3 we conclude that when two vortices are very close, a rapid, complete merger occurs, except when one of the vortices has such a small circulation compared to the other that complete straining out occurs. As the separation distance between the vortices increases at a constant circulation ratio, the interaction regimes that appear are partial merger, partial straining out, and elastic interaction. Although our resolution of the parameter space (Δ/R_1, R_2/R_1) is not sufficient to map out the detailed structure of the boundaries between regimes, we expect a gradual change of behavior when moving along a line of constant circulation ratio. The exception is the case of a completely symmetric interaction (i.e., $\zeta_2 = \zeta_1$, $R_2 = R_1$, and $C_2 = C_1$), where a

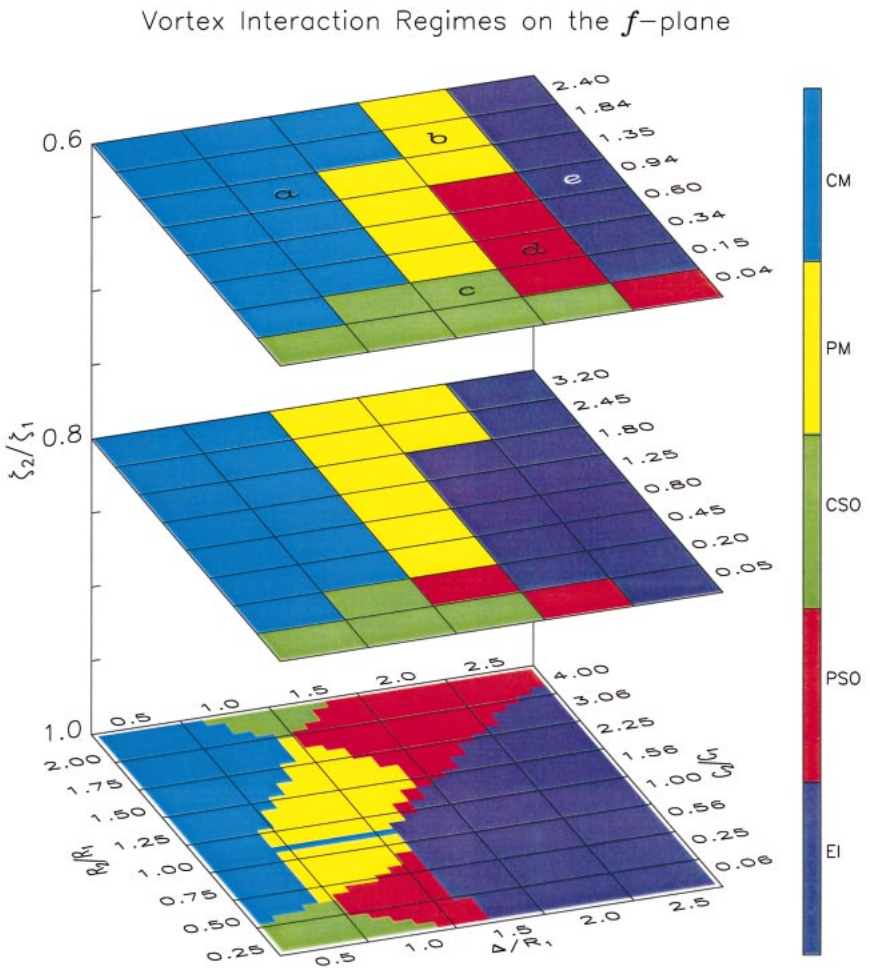

FIG. 3. Interaction regimes for binary vortices calculated as a function of the normalized separation distance Δ/R_1 and the radius ratio R_2/R_1 for (top) $\zeta_2/\zeta_1 = 0.6$, (middle) $\zeta_2/\zeta_1 = 0.8$, and (bottom) $\zeta_2/\zeta_1 = 1.0$. All calculations were performed on the f plane. The bottom surface is adapted from the contour surgery calculations of Dritschel and Waugh (1992). The letters shown in individual boxes on the upper surface refer to the experiments shown in Fig. 2.

bifurcation point is found near $\Delta/R_1 = 1.4$. In this case the identical nature of the two vortices prevents one from dominating the other, so that the intermediate regimes (PM, PSO) are not found, and the interaction goes from a CM to an EI within a very small neighborhood of the bifurcation point. In reality, a completely symmetric tropical cyclone binary interaction would be a very rare event, so that this bifurcation point, while of considerable theoretical interest, is of less practical interest. To gain some insight about the critical ratio of circulation for the transition from the bifurcation regime to the smooth regime, we made two complementary high-resolution runs (not shown) with four nested grids of 1024 × 1024 grid points each (see Table 2). The initial condition was two equally sized vortices ($R_1 = R_2$) with different vorticities and, therefore, different circulations (5% and 2% difference). These two experiments showed a clear partial merger, where the very small remnant of the weaker vortex was strained out shortly after it was detached.

TABLE 2. Same as Table 1, but for the high-resolution numerical experiments.

l	n_x	n_y	x_0 (km)	y_0 (km)	h_l (km)	Δt_l (s)
1	1024	1024	−6268.36	−6114.76	12.2429	276.92
2	1024	1024	−3134.18	−3139.74	6.1214	138.46
3	1024	1024	−1567.09	−1566.65	3.0607	69.23
4	1024	1024	−783.54	−782.98	1.5304	34.61

From Fig. 3 it can be seen that when one of the vortices is very intense (ζ_1 becoming significantly larger than ζ_2), its region of influence grows. For example, for a circulation ratio $C_2/C_1 = 0.5$, the elastic interaction regime is found near $\Delta/R_1 = 1.5$ when $\zeta_2/\zeta_1 = 1.0$, but it moves to $\Delta/R_1 = 2.0$ when $\zeta_2/\zeta_1 = 0.8$, and to $\Delta/R_1 = 2.5$ when $\zeta_2/\zeta_1 = 0.6$. This is consistent with the general notion that stronger hurricanes have a larger influence area than weaker hurricanes of the same size.

5. Differences between binary interactions on the f plane and the sphere

All of the 80 f-plane experiments shown in the upper two surfaces in Fig. 3 were also run on the sphere. For all the spherical runs the initial latitude of the vortex centers was 20°N. When these 80 spherical runs were classified and plotted on a diagram (not shown) similar to Fig. 3, it was found that the results are nearly identical to the f-plane results. Only in the three specific cases $(\Delta/R_1, R_2/R_1, \zeta_2/\zeta_1) = (1.5, 1.75, 0.6)$, (1.5, 1.75, 0.8), and (1.5, 2.0, 0.8) did the classification of Fig. 3 change from CM to PM for the first and from PM to CM for the other two. However, several differences in the flow evolution were detected. The case shown in Fig. 2b, which is classified as a PM, was chosen to describe the differences between binary vortex interaction on the f plane and on the sphere. In order to investigate this case in clearer detail, two additional runs, one on the f plane and one on the sphere, were performed with the resolution increased to 1024×1024 points on each of the four nested meshes (see Table 2 for further details). The diffusion coefficient for these higher-resolution runs was decreased to $\nu = 125\ \text{m}^2\ \text{s}^{-1}$.

Figure 4 shows the relative vorticity field for the spherical case with the parameters $\zeta_2/\zeta_1 = 0.6$, $\zeta_1 = 9.333 \times 10^{-4}\ \text{s}^{-1}$, $R_1 = 100$ km, $R_2 = 175$ km, and $\Delta/R_1 = 2.0$. The maximum wind speed produced by vortex 1 is 46.7 m s^{-1}, while the maximum wind speed produced by vortex 2 is 49.0 m s^{-1} (Fig. 5 shows the binary system meridional wind as a function of x at $t = 0$, $y = 0$, where the x domain corresponds to the outermost grid). The domain shown in Fig. 4 corresponds to the innermost (moveable) grid, and the x–y scales are those of the Mercator projection with origin at $(\phi, \lambda) = (20°\text{N}, 60°\text{W})$. At $t = 0$, the fluid surrounding the vortices has zero relative vorticity, shown in the figure as light-gray shading. As time progresses, the advection produced by the vortices and the conservation of absolute vorticity create β gyres, with the cyclonic gyre on the lower-left-hand side of the vortex pair (light-gray shading), and the anticyclonic gyre (white area) immediately around and to the north of the vortices. Because of the nonlinear evolution of the flow, the β gyres have a complicated behavior, constantly changing shape and orientation. These gyres are responsible for the translation of the binary system approximately 2000 km to the west and 1000 km to the north in 72 h. Both vortices were initially uniformly covered by passive air parcels that were advected by the flow. The tracers that were found inside vortex 2 at $t = 40$ h (Fig. 4c) were traced back to their original positions and are also shown at $t = 0$ (Fig. 4a). It is clear that the air eroded from vortex 2 came from its periphery, while the air initially at its center remains at the center of the vortex even after an aggresive and destructive interaction with the more compact vortex (Fig. 4b). This behavior was also observed in the f-plane case. It is well known from 2D turbulence experiments (McWilliams 1984), and from atmospheric observations and theories (Bowman 1996; McIntyre 1989), that high vorticity gradients protect vortex cores from violent interactions. However, an interesting aspect of this case is that the vorticity gradient inside the vortices is zero, so that it is not obvious that the center of the initially larger vortex should remain coherent, even after 72% of its vorticity has been removed in a complicated manner.

The separation distance between vortex centers as a function of time is shown in Fig. 6a, with the thick dashed line corresponding to the experiment evolving on the sphere (great-circle distance) and the thin dashed line to the experiment evolving on the f plane. During the first 12 h, the separation distance remains approximately constant. However, the shape of the larger vortex starts to show significant deformation as early as $t = 7$ h. After an approach of the centers around 18 h, there is a tendency for separation from about 25 to 47 h. This coincides with the strongest mass transfer from the broad vortex to the more intense vortex. This can be explained as a consequence of the f-plane vorticity centroid conservation principle: as mass is transferred toward one vortex, the vortices have to separate in order to compensate for the higher contribution of the stronger vortex to the vorticity centroid.

At $t = 63$ h, the separation distance between centers is about the same (600 km) for the spherical and f-plane cases. However, afterward, the vortex pair on the sphere undergoes an ''escape event,'' with the separation distance increasing by 150 km in 9 h. This escape coincides with the period in which the now smaller and weaker vortex 2 is captured by the cyclonic β gyre, as shown in Figs. 4d–f.

The rate of orbital rotation (Fig. 6b) has strong oscillations throughout the 72-h integration. On both the f plane and sphere there is a tendency toward a slower rotation rate as time increases. This is a consequence of the increasing separation distance between vortex centers, which causes a decrease of their mutual advection effect. The rotation rate for the case on the sphere is generally smaller than the rotation rate for the f-plane case because some of the energy of the spherical case is spent in a mutual translation of the vortices by the β effect. The final consequence of this slower rotation rate is that, by 72 h, the vortices on the sphere have rotated about 600° about their centroid, while the vortices on the f plane have rotated about 810°. A comparison of the vortex tracks for these experiments is shown in Figs. 6c (f plane) and 6d (sphere).

An additional difference between the f-plane and spherical cases is that, because of the absolute vorticity conservation, as the vortices move poleward of their original position (20°N) their strength (relative vorticity ζ) decreases in order to compensate for the increase in f. Although this is a small effect compared to the other effects mentioned above, it may have consequences after a PM when a very small vortex remains; this small

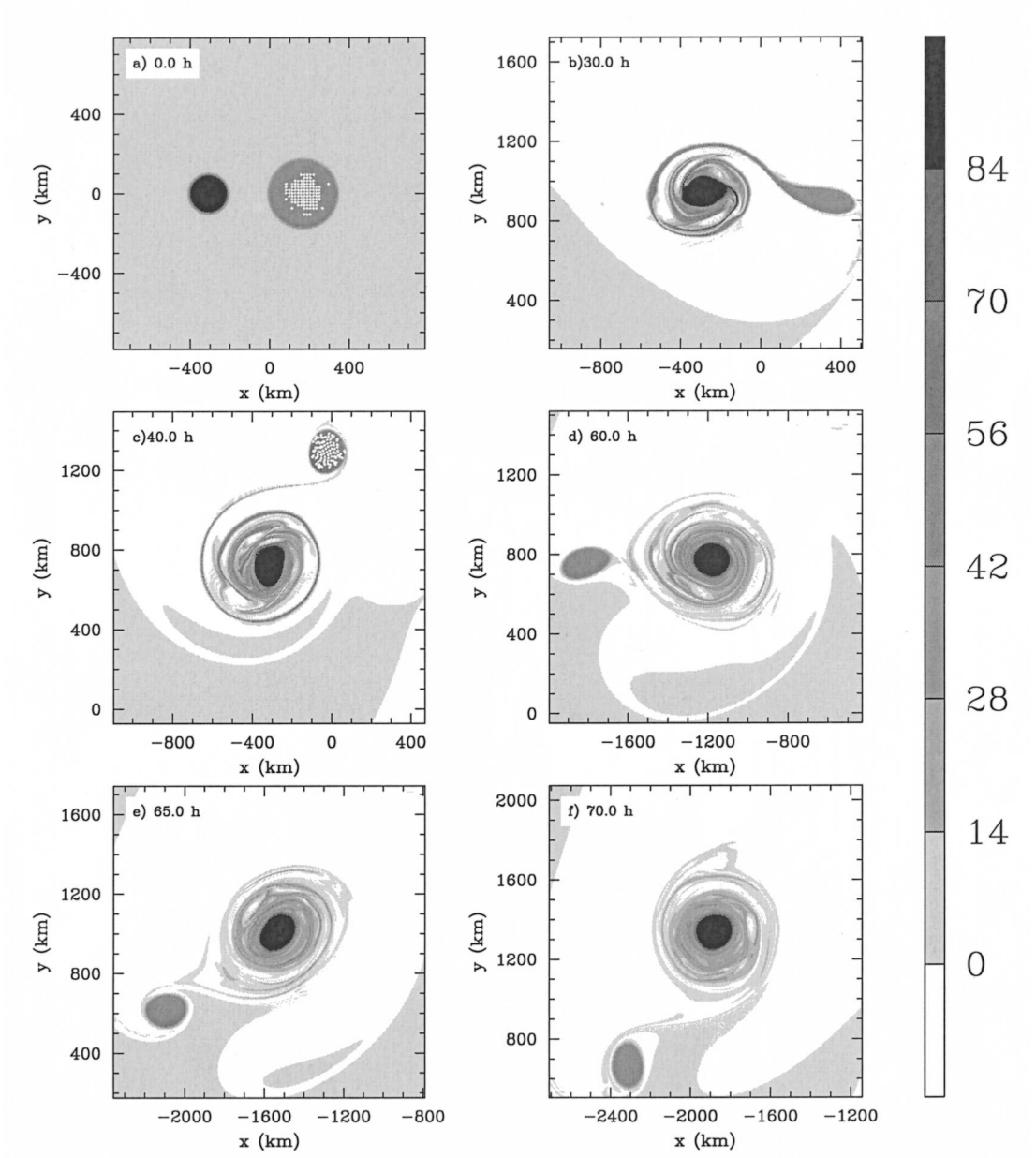

FIG. 4. Partial-merger experiment on the sphere at 1024 × 1024 resolution. The initial separation distance between the vortex edges is $\Delta = 200$ km, and the initial vorticity ratio is $\zeta_2/\zeta_1 = 0.6$, with $\zeta_1 = 93.33 \times 10^{-5}$ s^{-1}, $R_1 = 100$ km, and $R_2 = 175$ km. The numbers on the grayscale bar correspond to vorticity in units of 10^{-5} s^{-1}. The white dots shown inside the small vortex at $t = 40$ h were traced back to the initial time and are also shown at $t = 0$ h.

vortex is more easily eroded on the sphere than on the f plane.

6. Conclusions

The possible interactions between two tropical-cyclone-like vortices have been classified in this work. Two of the intermediate types of interaction (PM and PSO) have received little attention in the meteorological literature on binary tropical cyclone interactions. These deserve further observational study because of the complex interactions taking place. For example, during a partial merger, repeated mass exchanges can occur between vortices. These exchanges are an essential element in the behavior of the binary system and involve nonlinear effects, making very difficult an a priori quantification of the mass exchange without a direct numerical integration from a precise initial condition. It was observed that an increase in the separation distance between vortices can occur in both the spherical and the

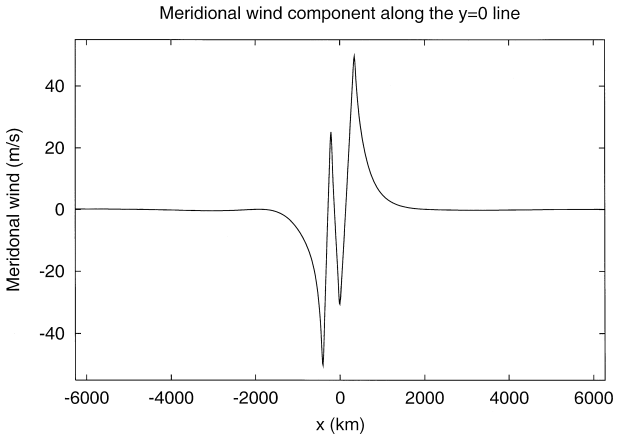

FIG. 5. Meridional wind as a function of x at $t = 0$, $y = 0$ for the binary system shown in Figs. 2b and 4a. The x domain corresponds to the outermost grid.

f-plane cases because of mass exchanges, but an escape due to capture by a third system (β-gyre) can only happen in the variable f case.

After a detailed analysis of the results summarized in this work, we hypothesize that partial mergers are quite frequent in binary tropical cyclone systems that overcome a period of mutual rotation but end up in an escape event. One classic example is seen in a famous visible image of the binary hurricane system comprised of Hurricanes Ione and Kirsten (1974) in the eastern Pacific (Larson 1975), where a cloud band seems to ''connect'' the cores of both hurricanes; however, the storms separated and escaped from one another.

In the above experiments and from the analysis of air parcel trajectories, it was observed that during a strong shearing event the vortex core is the most resistant region, even when the vorticity gradient inside the cyclone is zero. During partial-merger experiments in which a very small percentage of an initially broad vortex is left (less than 10%), the central region is the part that survives the violent interaction.

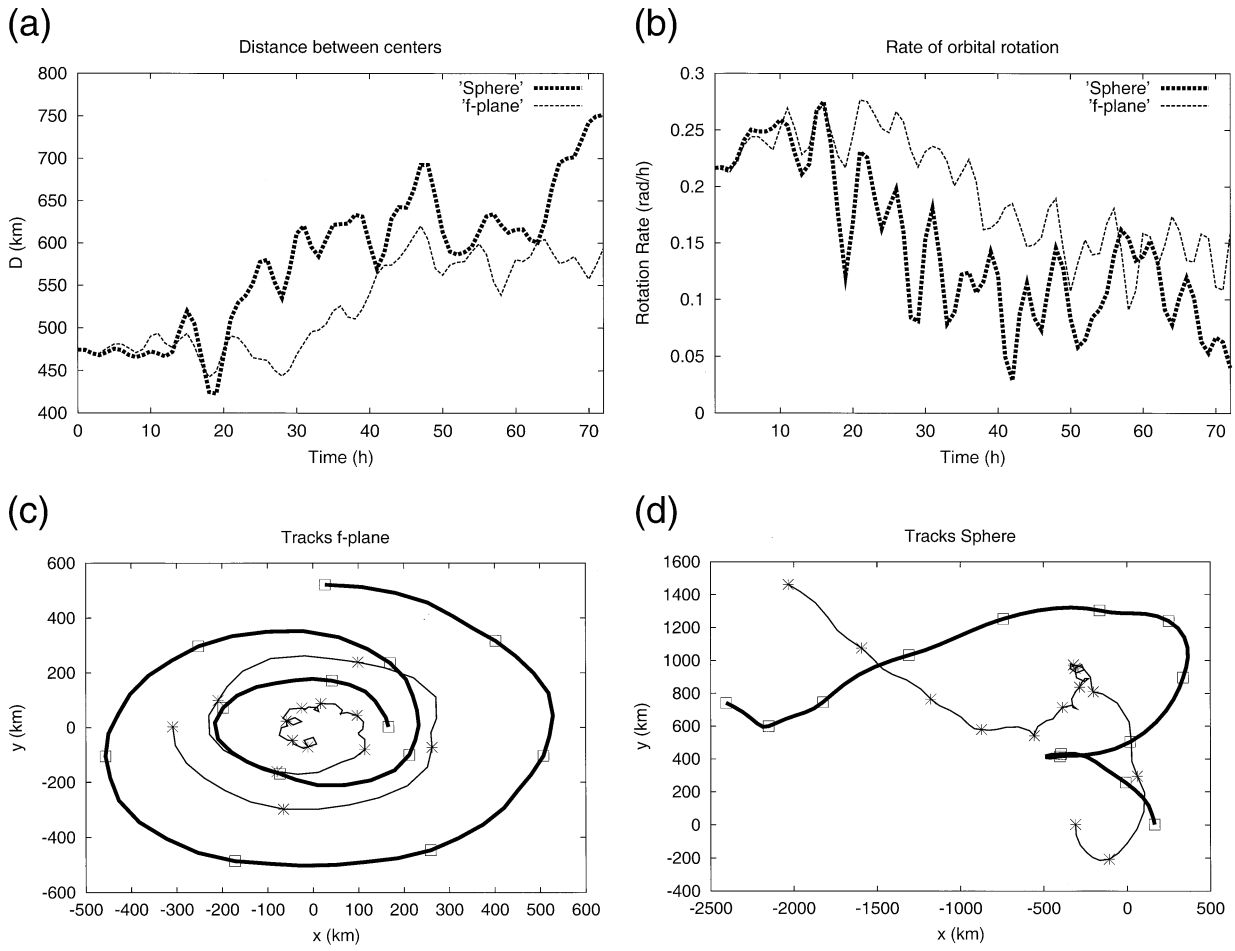

FIG. 6. Comparison between partial-merger experiments on the f plane (Fig. 2b) and on the sphere (Fig. 4): (a) separation distance between vortex centers, (b) rotation rate of the line joining the vortex centers, (c) tracks on the f plane, and (d) tracks on the sphere (Mercator projection). In (c) and (d), time marks are shown every 6 h.

As mentioned above, the size, shape, and location of the β gyres was highly variable during the 72 h of the experiments on the sphere. Those changes had important consequences on the actual tracks followed by the vortices. For example, in Fig. 6d the vortices initially moved in a northward direction, making a loop, moving westward, then northwestward, and finishing with an escape event. For this reason it seems fundamental that the characteristics of the β gyres (size, shape, strength, and orientation) should be fully included in the initial condition of any tropical cyclone simulation intended to forecast the movement of the storm.

Acknowledgments. We would like to thank Paul Ciesielski, Jonathan Vigh, Mark DeMaria, Richard Johnson, Michael Montgomery, and two anonymous reviewers for their comments and suggestions. This research was done while RP was a visiting scientist at the CSU Department of Atmospheric Science under the sponsorship of NOAA Grant NA67RJ0152. The other authors were supported by NASA/CAMEX Contract NAG5-11010, ONR Grant N00014-98-1-0103, and NSF Grant ATM-0087072.

REFERENCES

Bowman, K. P., 1996: Rossby wave phase speeds and mixing barriers in the stratosphere. Part I: Observations. *J. Atmos. Sci.*, **53,** 905–916.

Brand, S., 1970: Interaction of binary tropical cyclones in the western North Pacific Ocean. *J. Appl. Meteor.*, **9,** 433–441.

Chang, S. W., 1983: A numerical study of the interactions between two tropical cyclones. *Mon. Wea. Rev.,* **111,** 1806–1817.

Dritschel, D. G., 1988: Contour surgery: A topological reconnection scheme for extended integrations using contour dynamics. *J. Comput. Phys.*, **77,** 240–266.

——, and D. W. Waugh, 1992: Quantification of the inelastic interaction of unequal vortices in two-dimensional vortex dynamics. *Phys. Fluids,* **4A,** 1737–1744.

Fujiwhara, S., 1921: The natural tendency towards symmetry of motion and its application as a principle of motion. *Quart. J. Roy. Meteor. Soc.,* **47,** 287–293.

——, 1923: On the growth and decay of vortical systems. *Quart. J. Roy. Meteor. Soc.,* **49,** 75–104.

——, 1931: Short note on the behaviour of two vortices. *Proc. Phys. Math. Soc. Japan, Ser. 3,* **13,** 106–110.

Fulton, S. R., 1997: A comparison of multilevel adaptive methods for hurricane track prediction. *Electron. Trans. Numer. Anal.,* **6,** 120–132.

——, 2001: An adaptive multigrid barotropic tropical cyclone track model. *Mon. Wea. Rev.,* **129,** 138–151.

Holland, G. J., and G. S. Dietachmayer, 1993: On the interaction of tropical-cyclone-scale vortices. III. Continuous barotropic vortices. *Quart. J. Roy. Meteor. Soc.,* **119,** 1381–1398.

Kossin, J. P., and W. H. Schubert, 2001: Mesovortices, polygonal flow patterns, and rapid pressure falls in hurricane-like vortices. *J. Atmos. Sci.,* **58,** 2196–2209.

Kuo, H., G. Chen, and C. Lin, 2000: Merger of tropical cyclones Zeb and Alex. *Mon. Wea. Rev.,* **128,** 2967–2975.

Lander, M., and G. J. Holland, 1993: On the interaction of tropical-cyclone-scale vortices. I: Observations. *Quart. J. Roy. Meteor. Soc.,* **119,** 1347–1361.

Lansky, I. M., T. M. O'Neil, and D. A. Schecter, 1997: A theory of vortex merger. *Phys. Rev. Lett.,* **79,** 1479–1482.

Larson, R. N., 1975: Hurricane twins over the Eastern North Pacific Ocean. *Mon. Wea. Rev.,* **103,** 262–265.

McIntyre, M. E., 1989: On the Antartic ozone hole. *J. Atmos. Terr. Phys.,* **51,** 29–43.

McWilliams, J. C., 1984: The emergence of isolated coherent vortices in turbulent flow. *J. Fluid Mech.,* **146,** 21–43.

Melander, M. V., N. J. Zabusky, and A. S. Styczek, 1986: A moment model for vortex interactions of the two-dimensional Euler equations. Part 1. Computational validation of a Hamiltonian elliptical representation. *J. Fluid. Mech.,* **167,** 95–115.

Ritchie, E. A., and G. J. Holland, 1993: On the interaction of two tropical cyclone scale vortices. II: Discrete vortex patches. *Quart. J. Roy. Meteor. Soc.,* **119,** 1363–1379.

Schubert, W. H., M. T. Montgomery, R. K. Taft, T. A. Guinn, S. R. Fulton, J. P. Kossin, and J. P. Edwards, 1999: Polygonal eyewalls, asymmetric eye contraction, and potential vorticity mixing in hurricanes. *J. Atmos. Sci.,* **56,** 1197–1223.

Wu, C.-C., T.-S. Huang, W.-P. Huang, and K.-H. Chou, 2003: A new look at the binary interaction: Potential vorticity diagnosis of the unusual southward movement of Tropical Storm Bopha (2000) and its interaction with Supertyphoon Saomai (2000). *Mon. Wea. Rev.,* **131,** 1289–1300.